International Journal of Chemistry, Mathematics and Physics (IJCMP)
[Vol-6, Issue-3, May-Jun, 2022]
https://dx.doi.org/10.22161/ijcmp.6.3.1
ISSN: 2456-866X

Morphological, structural and electrochemical properties of the $LaNi_4Fe$ compound elaborated by mechanical alloying

M. Ben Moussa[1,2,*], A. Hakamy[1]. M. Abdellaoui[2]

[1]Physics Department, College of Applied Science, Umm AL-Qura University, Makkah, Saudi Arabia.
[2]Institut National de Recherche et d'Analyse Physico-chimique, Pôle Technologique de Sidi Thabet, 2020 Sidi Thabet, Tunisie.

Received: 22 Apr 2022; Received in revised form: 11 May 2022; Accepted: 15 May 2022; Available online: 21 May 2022

Abstract— *In this paper, we have studied the morphologic, the structural and the electrochemical properties of the $LaNi_4Fe$ compound elaborated by mechanical alloying (MA) for two durations 5 and 10 h. These properties are determined by various methods, such as XRD (X-ray Diffraction), SEM (Scanning Electron Microscopy) and galvanostatic cycling. The results show that the $LaNi_4Fe$ compound crystallizes in the hexagonal $CaCu_5$ type structure for the two alloying durations 5 and 10 h. The particles obtained by mechanical alloying are in the order of 6 to 7 nm. The chemical microanalysis by EDX (Energy Dispersive X-ray Spectroscopy) shows that the nominal and actual compositions are very close for the two grinding times. The maximum discharge capacity, of 180 and 200 mAh / g respectively for 5h and 10 h, is obtained from the first two cycles, which shows that the activation of nano compounds is easier than that obtained for bulk material obtained by melting since the reaction surface is larger. A decrease in capacity is observed after about thirty cycles: A loss of around 15% of maximum capacity is observed.*

Keywords— ***mechanical alloying, nanomaterials, structure, morphology, chronopotentiometry.***

I. INTRODUCTION

The intermetallic AB_5-type compounds are widely used for energy systems as solid state storage and electrochemical applications as negatives electrodes in NiMH batteries [1-2]. Among hydrogen storage systems, metal hydrides are considered to be one of the promising alternatives to satisfy the requirements for mobile application [3]. Among the intermetallic compounds of AB_5-type capable of absorbing hydrogen in a reversible manner, $LaNi_5$ and its derivatives ($La_{1-y}A_yNi_{5-x}M_x$ (A = Ce, Ca, mishmetal, and M = Fe, Co, Al,...) are by far the most studied. They have known for several years an important commercial use as negative electrode in "Ni-MH" batteries [4-5]. The partial substitution of nickel by other elements remarkably modifies the absorption properties of the compound, in particular the equilibrium pressure, the width hysteresis and the maximum capacity [6-7]. Young et al. [8], by combining the XRD, SEM and TEM (Transmission electron microscopy) studies, show that the disappearance of the crystalline peaks of $LaMgNi_4$ in the XRD pattern is due to a process of amorphization induced by hydrogen. Yang-huan et al. [9] studied the AB_5-type compound and showed that the substitution of Y for Sm improves significantly the de-hydriding rates of $REMg_{11}Ni - 5MoS_2$ (RE=Y, Sm) alloys, for which the reduction of dehydrogenation activation energy produced by substituting Sm with Y is responsible. Wanhai Zhou et al. [10], showed that after partial substitution of Ni by Mn in the $La_{0.78}Ce_{0.22}Ni_{4.4-x}Co_{0.6}Mn_x$ (x = 0 – 0.8) compound, both the hydrogen desorption capacity and the plateau pressure decrease, and correspondingly result in an improved thermodynamic stability which is adverse to low-temperature delivery [11-12].

Zhewen Ma et al. [13], investigated the size effects of the nickel powder additive on the low-temperature electrochemical performances and kinetics of $MmNi_{0.38}Co_{0.7}Mn_{0.3}Al_{0.2}$ hydrogen storage alloy under various assigned low temperatures. They [13] showed that the substitution of nano-nickel powder with average

particle size of 40 nm reduces the charge-transfer resistances and increases both the exchange current densities and the hydrogen diffusion coefficients of the electrodes more significantly than those of 100 nm at low temperatures. These enhancements were attributed to the excellent electro catalytic activity of 40 nm. Thus, the size of the particles has a good effect on the cycling and activation of the electrodes. The smaller the powders, the faster the electrochemical capacity is reached. In this work, mechanical alloying process was used in order to study the influence of the nanostructured state, obtained by this technique, on the structural, morphologic and electrochemical properties of the compounds. We have contented ourselves with developing a monosubstituted compound which is $LaNi_4Fe$. Two synthesis times 5 and 10 h were used to develop this compound.

II. EXPERIMENTS DETAILS

Mechanical alloying was performed using a Fritsch pulverisette P7 planetary ball mill. Five balls with 12 mm in diameter and 14 g in mass and 1.5 g of a mixture of lanthanum powder (99.9%), nickel (99.95%) and iron (99.98%) are introduced into a cylindrical container with a 45 ml volume in order to accomplish the mechanical alloying operation. The filling step is carried out under an argon atmosphere in a glove box. The containers are sealed in the glove box with Teflon gaskets. The ball mill was set at a disc rotation speed and a vial rotation speed equal respectively to 550 and 1100 rpm, These synthesis conditions correspond to a kinetic shock energy of 0.1 J / shock, a total shock frequency of 114.1 Hz and an injected shock power of 7.614 W/g. Two milling durations of 5 and 10 h were used during the synthesis of the $LaNi_4Fe$ compound.

The electrode was prepared by mixing the alloy powder crushed under argon atmosphere (90%) with carbon black (5 %) and PTFE solution (5%). Two pieces of 0.5 cm^2 of this latex were pressed on each side of a nickel grid to prevent the electrode plate from breaking during the charge–discharge cycling [14]. This set forms the negative electrode of Ni/MH accumulator. The counter electrode was formed by the Ni oxyhydroxide $Ni(OH)_2$, whereas the reference electrode was the Hg/HgO. The used electrolyte was KOH (1 M), prepared with deionized water.

III. MORPHOLOGICAL CHARACTERIZATION AND MICROANALYSIS OF CHEMICAL COMPOSITION:

Scanning electron microscopy was used to characterize the morphology and local composition of the synthesized powders. Figures 1 and 2 show secondary electron micrographs at different magnifications of the $LaNi_4Fe$ compound obtained respectively after 5 and 10 h of MA. We note that the powders exhibit a ductile character reflected by the absence of sharp fracture faces. Figures 1b and 2b show that the size of the grains, formed in most cases by clusters of nanoparticles as we will see by XRD, is less than 1 μm. The microanalysis of the composition was carried out in three different areas to get an average of the composition and to get an idea of the homogeneity of the composition. The results of microanalysis of the $LaNi_4Fe$ compound are shown in Figures 3 and 4 for the samples obtained respectively after 5 and 10 h of MA. These results are expressed in mass and atomic percentages. ZAF corrections to atomic number (Z), atomic absorption (A) and fluorescence (F) are also included.

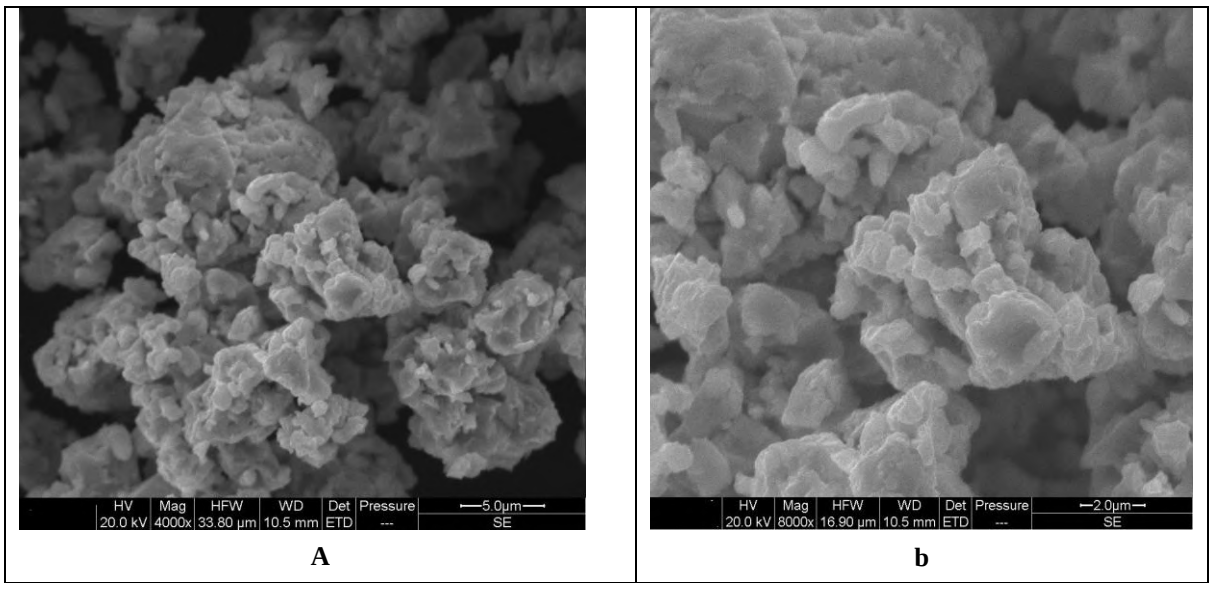

A **b**

Fig.1: SEM micrographs (secondary electrons mode) for e LaNi4Fe compound obtained after 5 h of milling: a) 4000X and b) 8000X

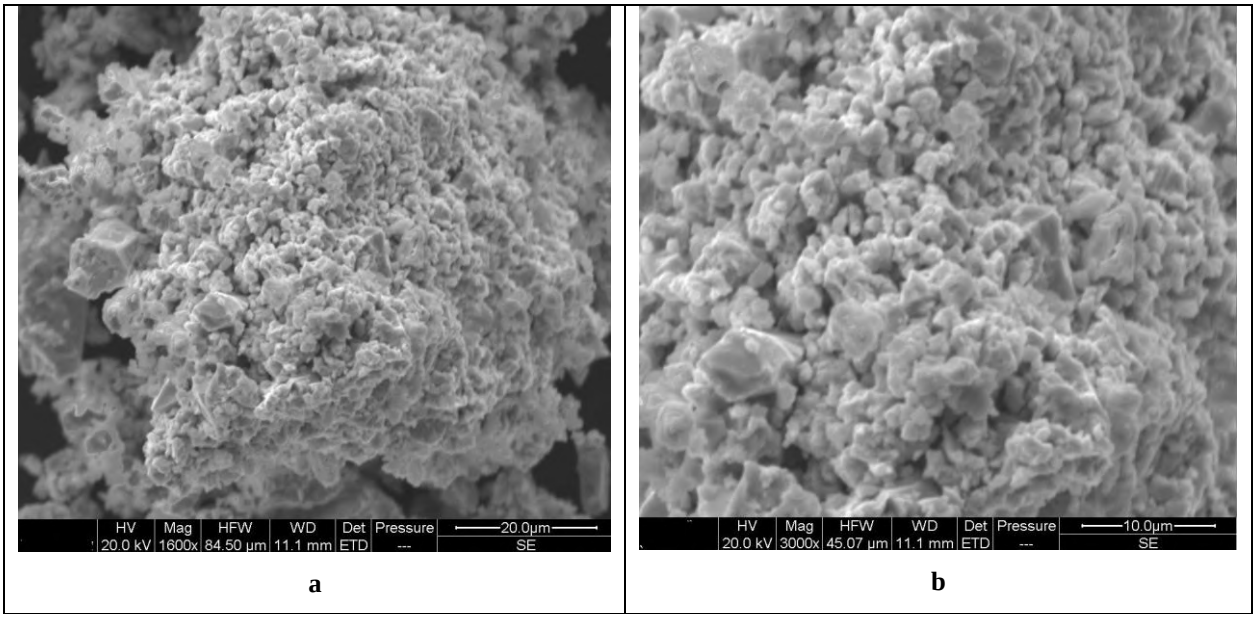

a **b**

Fig.2: SEM micrographs (secondary electrons mode) for the LaNi4Fe compound obtained after a period of 10 h for different magnifications: a) 1600 and b) 3000

The formula of the compound obtained after 5 h of MA is $La_{0.932}Ni_{3.579}Fe_{1.488}$. This composition exhibits an excess of iron relative to the nominal composition of the LaNi4Fe compound. This iron excess, which remains very low, is caused by the wear of balls and jars, made from stainless steel, during grinding. However, the compound obtained after 10 h of MA has the formula $La_{1.041}Ni_{3.9798}Fe_{0.9792}$ which is very close to the nominal composition of the compound $LaNi_4Fe$.

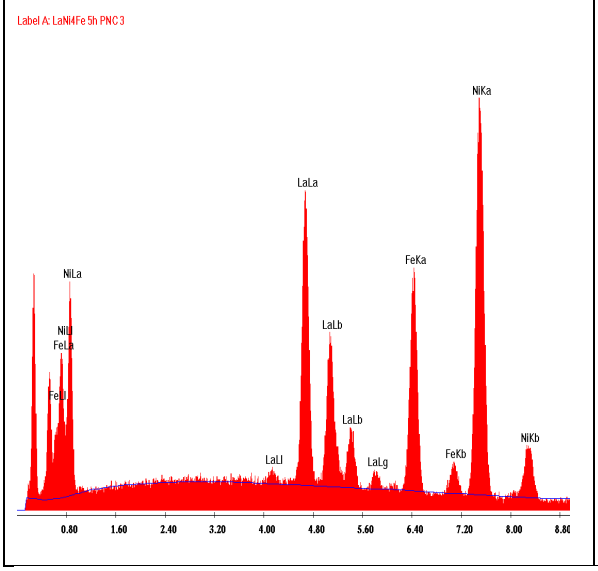

Elem	wt. %	at. %	K-ratio	Z	A	F
La	30.64	15.54	0.2878	0.8719	1.0363	1.0393
Fe	19.66	24.80	0.2016	1.0391	0.9260	1.0657
Ni	49.70	59.65	0.4913	1.0604	0.9321	1.0000
Total	100.0	100.0				

$La_{0.932}Ni_{3.579}Fe_{1.488}$

Fig.3: microanalysis of the $LaNi_4Fe$ compound obtained after 5 h of MA.

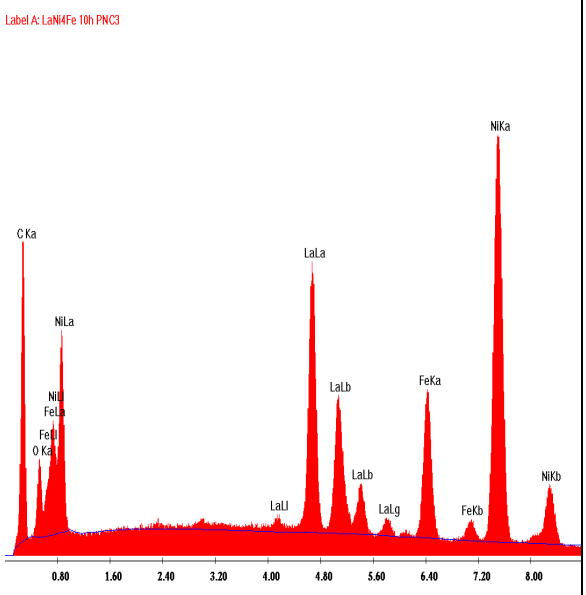

Elem	Wt. %	at. %	K-ratio	Z	A	F
La	33.40	17.35	0.3128	0.8749	1.0339	1.0354
Fe	12.63	16.32	0.1299	1.0430	0.9199	1.0721
Ni	53.97	66.33	0.5382	1.0646	0.9366	1.0000
Total	100.0	100.0				

$La_{1.041}Ni_{3.979}Fe_{0.979}$

Fig.4: microanalysis of the $LaNi_4Fe$ compound obtained after 10 h of MA.

IV. STRUCTURAL CHARACTERIZATION:

The structural properties of the $LaNi_4Fe$ compound were studied by X-ray diffraction. In order to calculate the lattice parameters and the grain size or the diffraction cristallite size (DCS), the FULLPROF program based on the Rietveld method was used to refine the XRD diffractograms of the $LaNi_4Fe$ samples obtained after 5 and 10 h of MA.

Figures 5 a and 5 b give the diffractograms of the $LaNi_4F$ compounds obtained respectively after 5 and 10 h, refined by the Fullprof program. These figures show a superposition of the experimental diffractogram (in red) and the calculated diffractogram (in black). The curve (in blue) gives the difference between the two diffractograms. A good refinement means a minimal difference between the calculated and measured values of intensity for all the points of the studied angular domain.

Tables 1 and 2 give the results of the XRD patterns refinements of the $LaNi_4Fe$ compounds synthesized respectively after 5 and 10 h of MA. The refinement results show that the diffraction crystallite sizes of the obtained particles are on the order of 6-7 nm. Likewise, we notice that when the grinding time increases from 5 to 10 h, the lattice parameter "c" and the lattice volume "V" decrease while the lattice parameter "a" remains almost constant. We believe that when the synthesis time increases, the material becomes denser as a result of the mechanical shocks to which it has been subjected. This induces a reduction in the volume of the unit cell by reducing one or more cell parameters. In this work, only the lattice parameter “c” decreases to have a reduction of the lattice volume. Moreover, the lattice volume obtained for these nanostructured compounds (87.808 $Å^3$) is lower than that of the less dense polycrystalline compounds obtained by UHF melting (89.173 $Å^3$) [15].

Iron has an atomic radius r_{iron} = 1.241 Å close to the atomic radius of nickel r_{nickel} = 1.246 Å and can theoretically be substituted in the two types of sites 2c and 3g. However, in this work good profile reliability factors (Rp), Bragg (RB) and therefore a good fit factor χ^2 are obtained when the Fe atoms substituted the Ni atoms in the 3g sites (in the plane z = 1/2). We believe this is due to two physical reasons: on the one hand, the 3g sites are located in the less dense z = 1/2 plane and can therefore harbor Fe atoms with minimum strain. On the other hand, it has been reported [16] that the substitution of Fe atoms in the 3g sites corresponds to a minimization of the total energy of the compound.

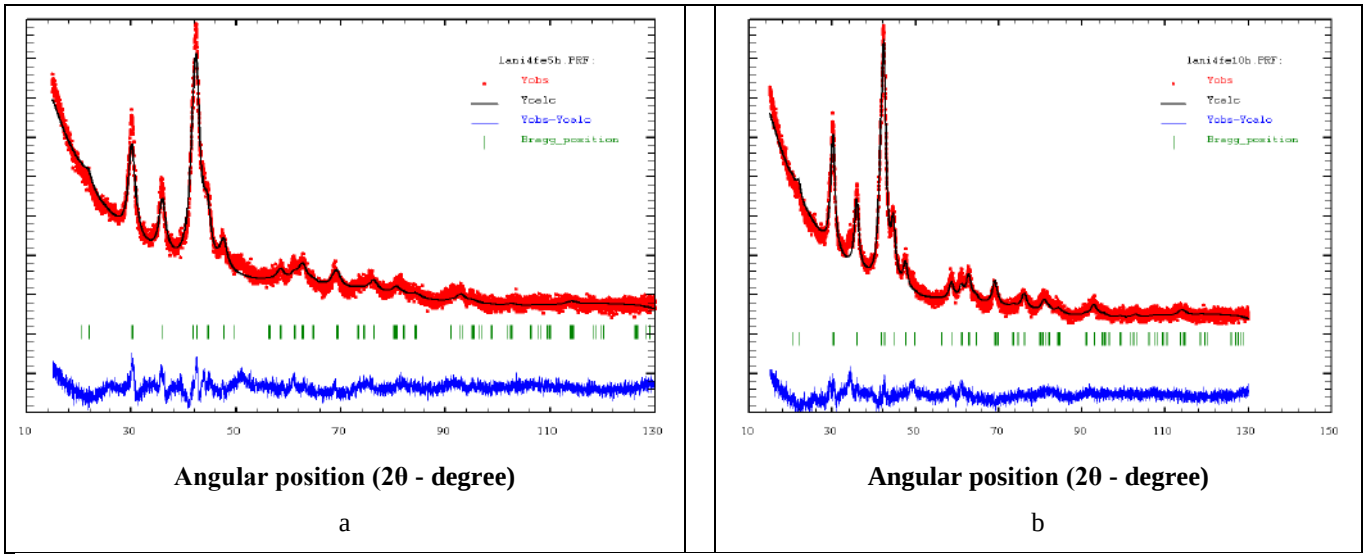

Fig.5: Rietveld refinement of the XRD pattern of the $LaNi_4Fe$ sample obtained after a) 5 h and b) 10 h of MA.

Table 1: Results of the refinement by the Fullprof program of the XRD pattern of the $LaNi_4Fe$ compound obtained after 5 h of MA.

Structure : $CaCu_5$-type Hexagonal Space group : P6/mmm Lattice parameters: a = b = 4.99236 Å, c = 4.06808 Å, V = 87.808 $Å^3$ α = β = 90°, γ = 120°						
Atomic positions:						
Atom	Type	Wyckoff Site	x	y	z	Occupation
La	La_1	1a	0	0	0	1
Ni	Ni_1	2c	1/3	2/3	0	2
Ni	Ni_2	3g	1/2	0	1/2	2
Fe	Fe_1	3g	1/2	0	1/2	1
Reliability factors: R_{wp} = 9.29 % Angular position (2θ - degree) R_{Bragg} = 6.44 % χ^2 = 2.56 Y = 1.5665 DCS = 6 nm						

Table 2: Results of the refinement by the Fullprof program of the XRD pattern of the $LaNi_4Fe$ compound obtained after 10 h of MA

Structure : $CaCu_5$-type Hexagonal Space group : P6/mmm Lattice parameters: a = b = 4.9984 Å, c = 4.0499 Å, V = 87.631 $Å^3$ α = β = 90°, γ = 120°						
Atomic positions:						
Atome	Type	Wyckoff Site	x	y	z	Occupation
La	La_1	1a	0	0	0	1

Ni	Ni_1	2c	1/3	2/3	0	2
Ni	Ni_2	3g	1/2	0	1/2	2
Fe	Fe_1	3g	1/2	0	1/2	1
Reliability factors: R_{wp} = 11.5 %			R_{Bragg} = 10.2 %		χ^2 = 2.64	
Y = 1.172			DCS = 7.5 nm			

V. ELECTROCHEMICAL MEASUREMENTS (LIFETIME CYCLE OF THE ELECTRODE):

All the electrochemical measurements were performed at room temperature in a conventional three-electrode open-air cell using VMP system. The discharge capacity of the electrode was determined by a galvanostatical charging–discharging at C/3 and D/6 regime, respectively. Every cycle was carried out by charging fully at 120 mA/g for 3 h (this time was majored by 50 % due to efficiency of the charging reaction) and discharging at 60 mA/g for 6 h at room temperature. Figure 6 gives the variation in the discharge capacity as a function of the number of cycles for the $LaNi_4Fe$ compounds obtained respectively after 5 and 10 h of MA. This figure shows that the maximum discharge capacity, of 180 and 200 mAh / g for respectively 5h and 10 h, is obtained after only the first two cycles. Unlike polycrystalline compounds which require several cycles to be activated, these results show that these nanomaterials obtained by mechanical alloying are easily activated. We believe that, unlike polycrystalline compounds, the obtained nanoparticles (6 to 7 nm) have a fairly large active surface area and therefore do not require any activation to reach maximum discharge capacity. These results show also that the substitution of nickel by iron improves the electrochemical discharge capacity. Indeed, Jurczyk et al. [17] developed by mechanosynthesis a nonsubstituted $LaNi_5$ compound and obtained a lower maximum discharge capacity of only 120 mAh/g, reached after two cycles of charge discharge. Figure 6 shows also that, after two cycles, the discharge capacity decreases when increasing the number of cycles. This decrease in capacity is attributed to the formation of oxidation layer and/or the corrosion of the material in the KOH solution. In fact, during cycling, the material undergoes successive expansions and contractions which lead to the decrepitation of the grains existing as clusters of nanoparticles (DCS = 7-6 nm). This phenomena increases the active surface area and therefore facilitates the insertion and diffusion of hydrogen into the volume of the material. However, the development of fresh active surfaces favors, depending on the chemical nature of the material, corrosion at the surface and the loss of the active material and consequently the decrease in discharge capacity. This decrease in capacity can also be attributed to the oxidation of the active surface and the formation of a barrier to the diffusion of hydrogen in the volume of the grains. Figures 7 and 8 give SEM micrographs (secondary electrons mode) and EDX microanalysis results after and before cycling corresponding to the latexes of the $LaNi_4Fe$ compound obtained respectively after 5 h and 10 h.

These figures show that after cycling, cracks are generated on the surface due to successive expansion and contraction during the absorption and desorption of hydrogen (decrepitation). This makes it possible to increase the reaction surface and to facilitate the phenomenon of corrosion in the presence of KOH solution. EDX microanalysis on the latex of the $LaNi_4Fe$ compound before and after cycling shows that after cycling, the oxygen content increases at the surface of the electrode, which proves the formation of certain oxides. These oxides generated on the surface of the negative electrode during cycling act as a barrier and prevent the diffusion of hydrogen atoms into the volume of the particles. This leads to a decrease in the electrochemical discharge capacity and consequently to a decrease in the life of the battery. This decrease in discharge capacity may also be due to a phenomenon of self-discharge by the dissolution of metallic elements.

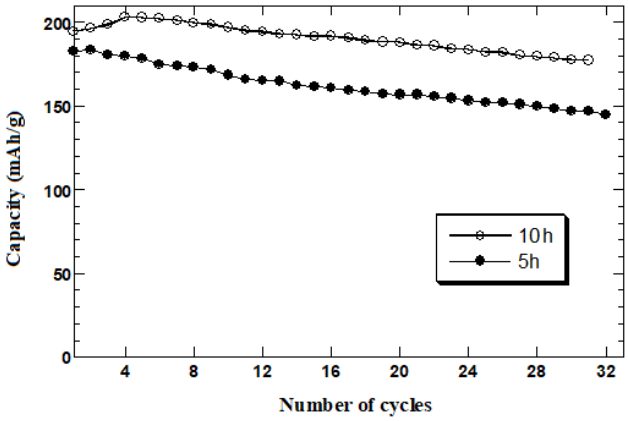

Fig.6: Variation of the electrochemical discharge capacity as a function of the number of cycles for the $LaNi_4Fe$ compound obtained by mechanical alloying after 5 and 10h.

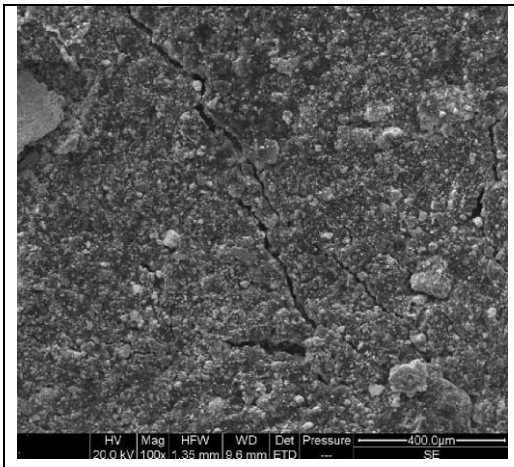

a

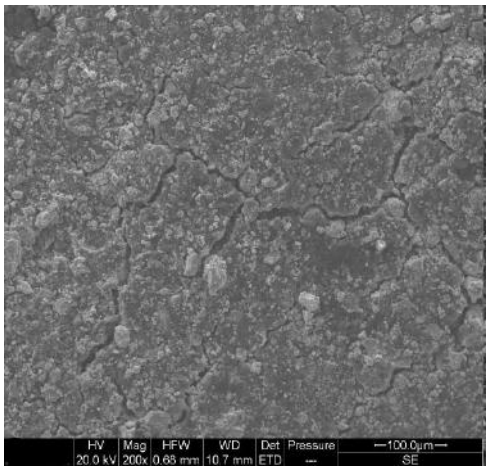

b

Elem	Wt. %	at. %	K-ratio	Z	A	F
C	52.23	81.53	0.1773	1.0752	0.3156	1.0001
O	2.16	2.53	0.0046	1.057	0.2011	1.0008
F	5.51	5.44	0.0169	0.9934	0.3082	1.0015
Si	0.11	0.08	0.0007	1.0126	0.5787	1.0007
La	13.32	1.8	0.114	0.7589	1.095	1.0293
Fe	7.16	2.4	0.0665	0.899	0.982	1.0523
Ni	19.51	6.23	0.1753	0.9135	0.9838	1.0000
Total	100.0	100.0				

Elem	Wt. %	at. %	K-ratio	Z	A	F
C	40.80	71.37	0.1255	1.0902	0.2822	1.0002
O	6.37	8.36	0.0149	1.0718	0.2182	1.0009
F	5.04	5.57	0.0151	1.0072	0.2975	1.0016
Al	0.65	0.51	0.0027	0.9974	0.4202	1.0006
Si	0.16	0.12	0.0009	1.0264	0.5398	1.0010
K	2.07	1.11	0.0190	0.9784	0.9250	1.0162
La	15.73	2.38	0.1346	0.7705	1.0816	1.0271
Fe	7.45	2.80	0.0695	0.9134	0.9722	1.0504
Ni	21.74	7.78	0.1973	0.9286	0.9772	1.0000
Total	100.0	100.0				

Figure 7: SEM micrographs (secondary electrons mode) and results of EDX microanalyses corresponding to the latexes of the $LaNi_4Fe$ compound obtained after 5 h of MA : a) before cycling and b) after cycling

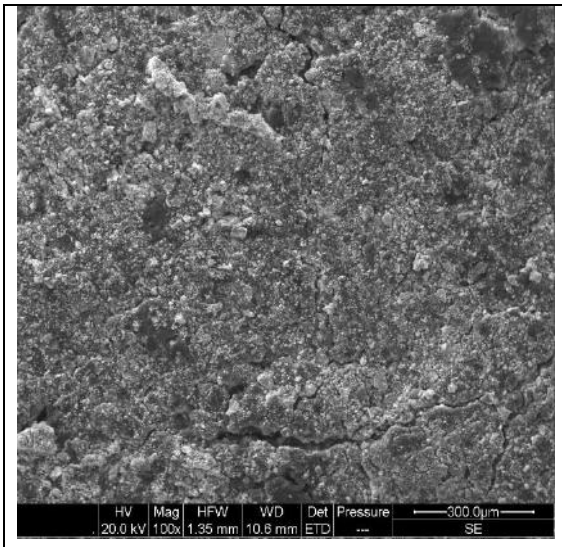

a

Elem	Wt. %	at. %	K-ratio	Z	A	F
C	43.17	74.07	0.1329	1.0900	0.2825	1.0002
O	2.52	3.25	0.0060	1.0715	0.2210	1.0010
F	9.02	9.79	0.0300	1.0070	0.3301	1.0016
Al	0.28	0.22	0.0012	0.9973	0.4161	1.0004
La	15.86	2.35	0.1365	0.7702	1.0873	1.0276
Fe	5.58	2.06	0.0525	0.9130	0.9740	1.0576
Ni	23.57	8.27	0.2145	0.9282	0.9806	1.0000
Total	100.0	100.0				

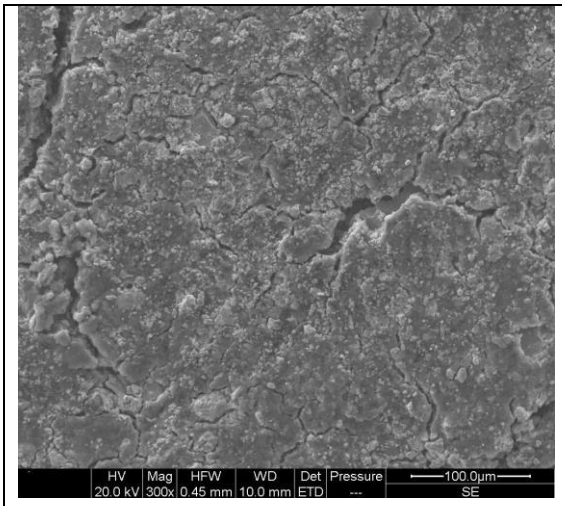

b

Elem	Wt. %	at. %	K-ratio	Z	A	F
C	48.83	75.19	0.1771	1.0668	0.3399	1.0001
O	6.11	7.06	0.0116	1.0488	0.1803	1.0007
F	5.74	5.59	0.0146	0.9857	0.2570	1.0011
Si	0.30	0.20	0.0019	1.0049	0.6189	1.0019
K	8.51	4.02	0.0787	0.9554	0.9574	1.0115
La	9.56	1.27	0.0791	0.7522	1.0778	1.0213
Fe	4.08	1.35	0.0375	0.8905	0.9837	1.0496
Ni	16.88	5.32	0.1509	0.9044	0.9889	1.0000
Total	100.0	100.0				

Fig.8: SEM micrographs (secondary electrons mode) and results of EDX microanalyses corresponding to the latexes of the $LaNi_4Fe$ compound obtained after 10 h of MA: a) before cycling and b) after cycling

VI. CONCLUSION

In summary, the following conclusions can be drawn;

1) The characterization by X-ray diffraction shows that the substitution of Ni by Fe retains the $CaCu_5$ structure and that the Fe atoms prefer the 3g sites (Z = ½) which corresponds to the most stable state for the compound;

2) The particles obtained by mechanical alloying have a size of the order of 6 to 7 nm;

3) The chemical analysis by SEM shows that the nominal and actual compositions are very close for the two grinding times;

4) The maximum electrochemical discharge capacity of the $LaNi_4Fe$ compound is of the order of 200 mAh / g, which is greater than that reported for the $LaNi_5$ compound produced by the same method (120 mAh / g);

5) A loss of around 15% of maximum discharge capacity is observed after about thirty cycles;

6) The activation of the obtained nanomaterials is easier than that of bulk material obtained by melting since the reaction surface is larger.

ACKNOWLEDGMENT

The authors would like to thank the Deanship of Scientific Research at Umm Al-Qura University for supporting this work by Grant Code 19-SCI-1-01-0032.

REFERENCES

[1] Ivan Romanov, Vasily Borzenko, Alexey Eronin, Alexey Kezakev, International Journal of Hydrogen Energy. https:// doi.org/10. 1016/ j. ijhydene. 2020. 10. 207.

[2] Marc Thele, Olivier Bohlen, Dirk Uwe Sauer, Eckhard Karden, Journal of power source 175 (2008) 635-643

[3] Yang-huan Zhang, Long-Wen Li, Dian-chen Feng, Peng-fei Gong, Hon-wei Shang, Shi-hai Guo, Transaction of Nonferrous Metals Society of China, 27 (2017) 551-561

[4] Wanhai Zhou, Zhengyao Tang, Ding Zhu, Zhewen Ma, Chaoling Wu, Journal Alloys and compounds 602 (2017) 364-374

[5] Priyanka Meena, Anoj Meena, Mukesh Jangir, V. K. Sharma, I. P. Jain, Materials Today: Proceeding 18 (2019) 901-911.

[6] K. D. Modibane, Lototskyy, M. W. Davids, M. Williams, M. J. Hato, K. M. Molapo, journal of Alloys and Compounds 750 (2018) 523-529

[7] Fikret Yilmaz, Semra Ergen, Soon-jik Hong, Orhan Uzum. International Journal of Hydrogen Energy 43 (2018) 20243-20253

[8] K. Young , T. Ouchi , H. Shen, L.A. Bendersky, international journal of hydrogen energy 40 (2015) 8941 – 8947.

[9] Yang-huan ZHANG, Wei ZHANG, Ze-ming YUAN, Wen-gang BU, Yan QI2, Xiao-ping DONG, Shi-hai GUO, Transaction of Nonferrous Metals Society of China 28(2018) 1828−1837

[10] Wanhai Zhou , Ding Zhu , Zhengyao Tang , Chaoling Wu, Liwu Huang , Zhewen Ma, Yungui Chen, Journal of Power Sources 343 (2017) 11-21

[11] L. Shcherbakova, M. Spodaryk, Yu. Solonin, A. Samelyuk, International Journal of Hydrogen Energy 38 (2016) 12133-12139

[12] K. young, B. Chao, Y. Liu, J. Nei, Journal of Alloys and Compounds 606 (2014) 97-104

[13] Zhewen Ma, Wanhai Zhou, Chaoling Wu, Ding Zhu, Liwu Huang, Qiannan Wang, Zhengyao Tang, Yungui Chen, Journal of Alloys and Compounds 660 (2016) 289-296

[14] Chuab-Jan. Li, Feng-Rong. Wang, Wen-Hao Cheng, Wei Li, Wen-Tong Zhoo, Journal Alloys Compounds 315 (2001) 218–223

[15] Sunil Kumar Pandey, Anchal Srivastava, O.N. Srivastava, International Journal of Hydrogen Energy 32 (2007) 2461 – 2465
[16] J. Lamloumi, A. Percheron-Guegan, C. Lartigue, J. C. Achard and G. Jehanno, Journal of the Less-Common Metals, 130 (1987) 111 - 122
[17] M. Jurczyk, M. Nowak, E. Jankowska, Journal of Alloys And Compounds, 340 (2002) 281-285.